

NASA Technical Paper 1248

LOAN COPY: RETURN TO  
AFWL TECHNICAL LIBRARY  
KIRTLAND AFB, N: M

TECH LIBRARY KAFB, NM  
034359

# Interaction of a Turbulent-Jet Noise Source With Transverse Modes in a Rectangular Duct

George P. Succi, Kenneth J. Baumeister,  
and K. Uno Ingard

JUNE 1978





NASA Technical Paper 1248

# Interaction of a Turbulent-Jet Noise Source With Transverse Modes in a Rectangular Duct

George P. Succi

*Massachusetts Institute of Technology, Cambridge, Massachusetts*

Kenneth J. Baumeister

*Lewis Research Center, Cleveland, Ohio*

K. Uno Ingard

*Massachusetts Institute of Technology, Cambridge, Massachusetts*

**NASA**

National Aeronautics  
and Space Administration

**Scientific and Technical  
Information Office**

1978

# INTERACTION OF A TURBULENT-JET NOISE SOURCE WITH TRANSVERSE MODES IN A RECTANGULAR DUCT

by George P. Succi, \* Kenneth J. Baumeister, and K. Uno Ingard<sup>†</sup>  
Lewis Research Center

## SUMMARY

A turbulent jet was used to excite transverse acoustic modes in a rectangular duct. The pressure spectrum showed asymmetric singularities (pressure spikes) at the resonant frequencies of the duct modes. This validates previously published theoretical results. These pressure spikes occurred over a range of jet velocities, orientations, and inlet turbulence levels. At the frequency of the spike, the measured transverse pressure shape matched the resonant mode shape.

In the experiment, the pressure response of a duct to an enclosed air jet was measured at frequencies from 0 to 25 kilohertz and from 0 to 5 kilohertz. The jet noise in these experiments was produced by drawing air through an orifice into a 3.81- by 10.16-centimeter ( $1\frac{1}{2}$ - by 4-in.) rectangular duct.

## INTRODUCTION

In the transmission of sound in a duct with or without flow, large amplitude variations in pressure can be produced by the interaction of the sound with the duct walls. For example, the combustor noise signature in a turbojet engine (such as recently reported in refs. 1 and 2) can be modified by the engine ducting. In those studies, the duct flow had some effect; nevertheless, the present study concentrates on the interaction of sound with duct walls in the absence of flow. Therefore, we used a turbulent jet to excite the transverse acoustic modes in a rectangular duct. Because the jet area was much smaller than the duct area, the duct flow was nearly zero and is thus neglected. The acoustic response to the jet near an eigenfrequency is identified, and the

---

\*Massachusetts Institute of Technology, Cambridge, Massachusetts.

<sup>†</sup>Professor of Physics, Massachusetts Institute of Technology, Cambridge, Massachusetts.

frequency range is determined for which the acoustic response in a duct differs qualitatively from the response in free space.

The qualitative acoustic response to turbulent jets in free space has long been known (ref. 3, pp. 123-125). In free space the sound pressure spectrum rises smoothly, approximately as the frequency squared, to a peak at a Strouhal number ( $St = \nu D/v_{\text{jet}}$ ) of about 0.2 (ref. 4); it then falls off smoothly, approximately as the inverse of the frequency squared. In a duct, however, the pressure spectrum of a jet is more complicated than for the same jet in free space.

Although the most popular model of the turbulent noise source of a free jet is a quadrupole (refs. 5 and 6), some success has been had in modeling the jet noise source as a distribution of simple (monopole) sources (ref. 7). Also, a turbulent field in the presence of boundaries has been shown to exhibit dipole source terms (ref. 6, ch. 3). If an enclosed jet can be modeled by a monopole source, the pressure spectrum theoretically (refs. 8 and 9) will show asymmetric singularities (pressure spikes) at the duct-mode cutoff frequencies.

Theoretically, the pressure spectrum of a fan noise source in a semi-infinite duct should show similar asymmetric spikes (ref. 6, p. 335). These spikes have been measured for a simulated fan noise source (ref. 10). Although they do not show the sharp spike at the resonant frequency predicted by theory, the measured spikes are asymmetric (ref. 10, fig. 8). In reference 10, however, detailed sound-pressure-level (SPL) traverses confirm that these peaks correspond to the excitation of higher order modes at the duct-mode resonant frequencies. Since both fan and jet noise sources can be modeled by simple acoustic sources, the simple source model should predict the response of a turbulent jet in a duct.

The main purpose of this study was twofold: First, to confirm the existence of asymmetric resonance peaks in the acoustic spectrum of an enclosed turbulent jet, to show that the simple source model adequately predicts the resonant frequencies, and to identify the acoustic modes associated with resonance; second, to study the effects of jet velocity, orifice diameter and orientation, Strouhal number, and inlet turbulence. These experiments were performed in a new flow-duct facility; therefore, a secondary purpose is to document the facility and instrumentation. Also, some important aspects of pressure measurements peculiar to duct acoustics are discussed as an aid in interpreting flow-duct data.

The pressure response of a duct to an enclosed turbulent jet was measured at frequencies of 0 to 25 kilohertz. The jet noise was produced by drawing air through orifices of different sizes and orientations at different flow rates.

## SYMBOLS

$A_d$  cross-sectional area of duct,  $m^2$

a	radius of sphere about a simple source, m
b	duct width, m
$c_0$	speed of sound, m/sec
D	orifice diameter, m
d	duct height, m
i	$\sqrt{-1}$
k	wave number (see eq. (6)), $m^{-1}$
$k_{mn}$	axial propagation coefficient for mode number (m, n), $m^{-1}$
$k_0$	source wave number of a propagating mode (see fig. 7 and eq. (18))
L	length of pipe, m
M	Mach number, $v_{jet}/c_0$
$M_P$	Mach number in pipe leading to orifice
m	transverse horizontal wave number
N	number of propagating modes
$\Delta N$	number of propagating modes in $\Delta\nu$
n	transverse vertical wave number
$n_t$	normal to wall
P	acoustic pressure, Pa
$P_{ref}$	reference rms pressure, Pa
$P_{rms}$	rms pressure (see eq. (10)), Pa
R	radiative resistance of source, g/sec
$S_w$	source strength, $m^3/sec$
St	Strouhal number, $\nu D/v_{jet}$
SPL	sound pressure level
T	one period of oscillation, sec
t	time, sec
v	velocity, m/sec
$v_d$	duct velocity, m/sec
$v_{jet}$	velocity of jet, m/sec
x	transverse horizontal duct coordinate, m

$y$	transverse vertical duct coordinate, m
$z$	axial duct coordinate, m
$\delta_{ij}$	Kronecker delta symbol (1 when $i = j$ ; 0 when $i \neq j$ )
$\kappa_n, \kappa_{m,n}$	eigenvalue (transverse mode in duct), $1/m$
$\Lambda_{mn}, \Lambda_n$	mean-square amplitude of cross-duct mode
$\lambda$	wavelength, $c_0/\nu$ , m
$\nu$	frequency, Hz
$\nu_{mn}, \nu_n$	cutoff frequency, $c_0/2\sqrt{(m/b)^2 + (n/d)^2}$ , Hz
$\nu_s$	Strouhal frequency, Hz
$\Delta\nu$	frequency interval, Hz
$\rho_0$	atmospheric density, $g/m^3$
$\psi_{mn}, \psi_n$	wave function
$\omega$	angular frequency, $2\pi\nu$ , rad/sec

## THEORY

A sound wave propagating in a rectangular duct can be composed of a fundamental plane wave and various transverse waves that depend on the nature of the noise source. The fundamental plane wave, identified as the (0, 0) mode, travels in the axial direction and has a uniform pressure distribution across the duct cross section. A transverse wave, identified as the (m, n) mode, has a nonuniform pressure distribution across the duct; consequently, it reflects back and forth from the duct walls as it travels along the duct.

The maximum number of modes in a sound wave propagating in a hard-wall duct depends on the frequency. For a given mode (i. e., the (m, n) mode) to propagate, its frequency must be greater than the duct "cutoff" frequency. However, a noise source may not excite (at significant magnitude) the maximum number of modes that its frequency content would indicate. For example, a loudspeaker that fills the entire duct end might excite a large-amplitude plane wave but greatly reduced-amplitude higher order modes. In any case, as the frequency of the source is increased beyond the mode cutoff frequency, a new mode becomes available for the radiation of sound down the duct.

The cutoff frequency for each mode and the pressure response of a simple (monopole) source in a duct are well known from classical acoustics (ref. 8, pp. 497-502). The classical theory relating to mode cutoff frequency and pressure response is briefly

reviewed here as a background for the experimental results.

### Cutoff Frequency

Consider a rectangular duct of width  $b$  and height  $d$ . The wave equation describing the propagation of an acoustic disturbance in a source-free region with negligible mean flow is

$$\nabla^2 P - \frac{1}{c_0^2} \frac{\partial^2 P}{\partial t^2} = 0 \quad (1)$$

where viscous effects have been neglected.

Because of the hard walls the normal particle velocity must be zero, which is equivalent to requiring

$$\left. \frac{\partial P}{\partial n_t} \right|_{\text{walls}} = 0 \quad (2)$$

where  $n_t$  is the normal to the wall. The axes of the Cartesian coordinate system are chosen so that the walls are located at  $x = 0, b$  and  $y = 0, d$ , as shown in figure 1.

For a sinusoidal time disturbance  $e^{-i\omega t}$ , the solutions to equation (1) are of the form

$$P(x, y, z, t) = \sum_m \sum_n A_{mn} \psi_{mn}(x, y) e^{ik_{mn}z} e^{-i\omega t} \quad (3)$$

where

$$\psi_{mn}(x, y) = \cos\left(\frac{m\pi x}{b}\right) \cos\left(\frac{n\pi y}{d}\right) \quad (4)$$

$$k_{mn} = \left(k^2 - \kappa_{mn}^2\right)^{1/2} \quad (5)$$

$$k = \frac{\omega}{c_0} \quad (6)$$

$$\kappa_{mn}^2 = \left(\frac{m\pi}{b}\right)^2 + \left(\frac{n\pi}{d}\right)^2 \quad (7)$$

and  $A_{mn}$  is an arbitrary constant. The functions  $\psi_{mn}$  are orthogonal to one another; that is,

$$\int_{\text{Area}} \psi_{mn}(x, y)\psi_{pq}(x, y)dx dy = \delta_{mp}\delta_{nq}A_d\Lambda_{mn} \quad (8)$$

where  $A_d$  is the cross-sectional area of the duct and  $\Lambda_{mn}$ , the average value of  $\psi_{mn}^2(x, y)$ .

The experiments were concerned with the excitation and propagation of the modes represented by the function  $\psi_{mn}$  as they travel down a duct. In particular, pressure traverses in the x-direction were made to determine if the  $\psi_{00}$ ,  $\psi_{10}$ , and  $\psi_{20}$  modes were present. The pressure amplitude (spatial) distribution of the first three modes is shown in figure 2. The plus and minus signs on the duct cross sections in figure 2 indicate the spatial domain when the  $\psi_{mn}$  term takes on either a positive or a negative sign. (The  $\psi_{mn}$  term is defined in eq. (4).) Recall from equation (3) that the pressure  $P$  also varies harmonically, as  $e^{-i\omega t}$ . The temporal variation of the  $\psi_{10}$  mode is shown in figure 3. Although a microphone will respond to this instantaneous variation in pressure, a typical measurement system records pressures in terms of the sound pressure level (SPL), defined as

$$\text{SPL} = 10 \log_{10} \frac{P_{\text{rms}}^2}{P_{\text{ref}}^2} \quad (9)$$

where  $P_{\text{rms}}$  is the rms (root mean square) sound pressure defined as

$$P_{\text{rms}} = \sqrt{\frac{1}{T} \int_0^T P^2 dt} \quad (10)$$

where  $T$  is one period of oscillation. The reference rms pressure  $P_{\text{ref}}$  is  $2 \times 10^{-5}$  pascal.

Assume, for example, that only one higher order mode is excited. Then substituting the product of  $\psi_{m,n}$  and the real component of  $e^{-i\omega t}$  into equations (9) and (10) yields the following SPL dependence on cross section:

$$\text{SPL} = \text{Constant} + 10 \log_{10} \left[ \cos\left(\frac{m\pi x}{b}\right) \cos\left(\frac{n\pi y}{d}\right) \right]^2 \quad (11)$$

The pressure amplitude (spatial) and SPL variations of the first three modes are shown in figure 4. The minimum sound pressure levels in figure 4(b) correspond to the dashed partition lines in figure 2. These types of SPL distributions indicate the presence of a particular mode. (The SPL is not, in general, equal to the intensity level in a duct if higher order modes are excited (ref. 9).)

We now replace the double index  $mn$  by the single index  $n$  by arranging the modes in order of increasing  $\nu_{mn}$ . From equation (5), for the  $n^{\text{th}}$  mode to propagate down the duct,  $k_n$  must be real. For a given frequency  $\nu$ ,  $k_n$  is real only if (ref. 3, p. 504)

$$\nu > \nu_n \equiv \frac{c_0 k_n}{2\pi} \quad (12)$$

where  $\nu_n$  is the cutoff frequency. That is, for any frequency, only a finite number of modes can propagate. To put it another way, each mode has a cutoff frequency: For frequencies below cutoff, the mode attenuates exponentially; for frequencies above cutoff, the mode propagates along the duct without attenuation. These ideas are illustrated in figure 5 for a modal pattern in a rectangular duct. The upper schematic shows decay,  $\nu < \nu_n$ ; the lower schematic shows propagation,  $\nu \geq \nu_n$ . Dissipative mechanisms can cause some attenuation in the propagating wave.

### Impedance of a Simple Source

The pressure near a simple source and the pressure radiated down the duct are directly proportional to the mechanical resistance at the source. However, the duct walls reflect sound back on the source and thus modify that resistance. The mechanical impedance of a point source inside a duct is discussed in the following paragraph.

Consider the response of a medium in a duct of cross-sectional area  $A_d$  to a simple (monopole) source of strength  $S_w$  and frequency  $\nu$ . The acoustic velocity is uniformly radial at a spherical surface of radius  $a$  ( $a \ll \lambda$ ) that just encloses the generating mechanism. The mechanical resistance of such a source in a duct can be shown to be (ref. 8, p. 502, eq. (9.2.12))

$$R = \rho_0 c_0 \frac{8\pi^2 a^4}{A} \left[ 1 + \sum_{n=1}^N \frac{k}{k_n} \frac{\psi_n^2(x_0, y_0)}{\Lambda_n} \right] \quad (13)$$

where the source is at the cross-sectional coordinate point  $(x_0, y_0)$ . The summation in equation (13) includes only the propagating modes, the last of which mode is labeled N.

To gain some insight into equation (13), we rewrote it for three ranges of the frequency  $\nu$  (recall that  $\nu_n$  represents the cutoff frequency):

For  $0 < \nu < \nu_1$ :

$$R = \frac{\rho_0 c_0^8 \pi^2 a^4}{A_d} \quad (14)$$

For  $\nu_1 \leq \nu < \nu_2$ :

$$R = \frac{\rho_0 c_0^8 \pi^2 a^4}{A_d} \left[ 1 + \frac{k}{k_1} \frac{\psi_1^2(x_0, y_0)}{\Lambda_1} \right] \quad (15)$$

For  $\nu_2 \leq \nu < \nu_3$ :

$$R = \frac{\rho_0 c_0^8 \pi^2 a^4}{A_d} \left[ 1 + \frac{k}{k_1} \frac{\psi_1^2(x_0, y_0)}{\Lambda_1} + \frac{k}{k_2} \frac{\psi_2^2(x_0, y_0)}{\Lambda_2} \right] \quad (16)$$

and so forth, as  $\nu$  increases.

A discontinuity (pole) appears in R as each cutoff frequency is crossed, since

$$k_n = \left[ \left( \frac{\omega}{c_0} \right)^2 - \kappa_n^2 \right]^{1/2} = \frac{2\pi}{c_0} (\nu^2 - \nu_n^2)^{1/2} = 0$$

for  $\nu = \nu_n$ . As  $\nu$  increases beyond  $\nu_n$ , the mechanical, or equivalently the radiative, resistance R drops as  $k_n^{-1}$ . When  $\nu$  increases above a new eigenfrequency, another pole is included in the expression for the resistance.

Figure 6 illustrates these resistance characteristics for an example taken from reference 8. As shown in figure 6, when the frequency of a simple source in a duct just equals the cutoff frequency, the theoretical radiation resistance increases step-wise and then decreases slowly as the frequency goes beyond cutoff. The number by each peak is the mode number (defined in eq. (4)). The dashed curve is the radiative resistance of the same source in free space.

## Pressure Response of a Simple Source

As mentioned, the pressure on the source and the pressure radiated to the far field are directly proportional to the resistance  $R$ . However, real fluid effects - such as energy dissipation by viscous friction, and thermal conduction - limit the pressure response at a cutoff frequency to a finite value and increase the bandwidth. Nonetheless, discrete jumps should occur at the cutoff frequency.

As the frequency of the source increases (eq. (13) and fig. 6), mechanical resistance increases in discrete jumps, each jump corresponding to an additional propagating mode. As  $\omega$  becomes large, the number of propagating modes added per unit change in  $\omega$  becomes larger, the interval between modes becomes shorter, and the peaks become narrower. At the high-frequency limit (ref. 8, p. 503),

$$\lim_{\omega \rightarrow \infty} \langle R \rangle = \rho_0 c_0 (4\pi a^2) k^2 a^2 \quad (17)$$

The average resistance is the radiative resistance of a source in free space. Consequently, at high frequencies the pressure response of a source in a duct approaches the response of the same source in free space.

For example, consider a rectangular duct - the geometry used in these experiments. The high-frequency limit of the radiative resistance is based on the number of modes available for sound propagation. Therefore, counting these modes gives some insight into their distribution with frequency.

The central effect is the phenomenon of mode cutoff. Cutoff can be discussed in terms of the characteristic mode wave numbers  $\kappa_{m,n}$ . Recall that the wave number is the angular frequency  $\omega$  divided by the speed of sound  $c_0$ . A mode propagates (does not exponentially decay) only if the source wave number  $k_0 = \omega/c_0$  is greater than or equal to  $\kappa_{m,n}$  (cutoff value of  $k$ ) as given in equation (7).

The problem is illustrated graphically by figure 7. The mode wave numbers are indicated by dots on a wave number graph (fig. 7(a)) and by a bar on the wave number - frequency plot (fig. 7(b)). For a mode to propagate, it must be included in the pie-shaped region described by radius  $k_0$  (fig. 7(a)). The total number of modes in this region is given by the number in the center of the pie-shaped region plus the number along each axis (ref. 8, p. 586), which is approximately

$$N = \frac{\pi}{4} \frac{k_0^2}{\left(\frac{\pi}{b} \frac{\pi}{d}\right)} + \frac{k_0}{\left(\frac{\pi}{b}\right)} + \frac{k_0}{\left(\frac{\pi}{d}\right)} \quad (18)$$

It is also useful to note how many new modes are available per unit increase in wave number  $\Delta k_0$ . Graphically, the number of modes added at a given frequency is proportional to the area of the quarter annulus surrounding the pie-shaped region. Obviously, this area is directly proportional to the source wave number  $k_0$ . From equation (18), the number of new modes that can propagate  $N$  per unit increase in  $k_0$  is

$$\frac{\Delta N}{\Delta k_0} = \frac{N(k_0 + \Delta k_0) - N(k_0)}{\Delta k_0} \approx \frac{\pi k_0}{2 \left( \frac{\pi}{b} \frac{\pi}{d} \right)} + \frac{1}{\left( \frac{\pi}{b} \right)} + \frac{1}{\left( \frac{\pi}{d} \right)} \approx \frac{\pi}{2} \frac{k_0}{\left( \frac{\pi}{b} \frac{\pi}{d} \right)} = \frac{\pi^2}{c_0} \frac{\nu}{\left( \frac{\pi}{b} \frac{\pi}{d} \right)} \quad (19)$$

At small wave numbers (frequencies),  $\Delta N/\Delta k_0$  is small; thus the frequency interval between the cutoff mode and the next propagating mode is large. At large wave numbers,  $\Delta N/\Delta k_0$  is large; thus the frequency interval between the cutoff mode and the next propagating mode is small. Equation (19) shows that  $\Delta N/\Delta k_0$  is directly proportional to frequency.

Experimental evidence of pressure spikes in a duct can be found only in the low-frequency range. Here the separation between modes is great enough to exhibit the asymmetric shape of the pressure spike. In the high-frequency range, neighboring modes overlap and obscure the shape of the pressure spikes. Pressure spikes are not observed at high frequencies since the bandwidth of a given pressure spike is much wider than the frequency interval between modes. The bandwidth of a spike (fig. 6) may be widened by energy dissipation. Thus, spike overlap is a consequence of the duct's acoustical properties. Increasing the frequency resolution of the detecting system therefore may not reveal any pressure spikes.

#### Theoretical Verification

Various theories have been postulated for the mechanisms by which jets generate sound: for example, the quadrupole, dipole, and monopole theories. In a recent presentation (abstracted in ref. 11), Powell pointed out that the various theories have led to interesting and apparently divergent views of the noise-generating source. However, regardless of the source, the present experiment should have revealed asymmetric pressure spikes at the "low" cutoff frequencies and a blending of the pressure into the free-space pressure response at the "high" frequencies. The reason is that pressure spikes depend primarily on the propagation characteristics of the medium and only secondarily on the noise source. For example, a dipole can be considered as two monopoles,  $180^\circ$  out of phase, separated by a small distance. Each monopole radiates as if the other was not there, and the radiative field is the sum of the two - asymmetric spikes and all.

## APPARATUS AND PROCEDURE

To verify the theory, we first placed a simple, broadband, noise source capable of exciting all the modes inside an infinitely long, hard-wall duct and then monitored the pressure spectrum for the characteristic asymmetric pressure spikes at the duct cutoff frequencies. The flow-duct system shown in figure 8 was adapted to simulate this idealized infinite-duct situation. The following paragraphs described this flow-duct system: first, the general operation; then, the key system components, in detail.

As shown in figure 8, a flow duct was connected by a 15-centimeter- (6-in. -) diameter vertical pipe into the NASA Lewis 1.2-meter- (48-in. -) diameter altitude exhaust header. The exhaust system has a nominal 68 940-pascal (20-in. -Hg) pressure at this point. The system was placed on line by first activating the 15-centimeter- (6-in. -) diameter remote-electric-motor valve directly beneath the 1.2-meter- (48-in. -) diameter header line and then opening the pneumatically adjustable, 15-centimeter- (6-in. -) diameter butterfly valve at the upper end of the vertical pipe.

Sound is generated by pulling room air through a small inlet orifice in the test section. The advantage of this suction system is that any turbulence in the flow is induced solely by the inlet orifice. In contrast, a compressed-air system would require a large settling tank to insure uniform flow conditions. And a settling tank would require acoustic treatment to prevent the excitation of resonant modes (ref. 12).

In the suction system the air jet passing through the orifice into the duct is sufficient to generate a strong (80 to 130 dB) noise source with the characteristic jet spectrum. However, the small-orifice jet diffuses into the large duct in such a way that the duct Mach number effects are negligible. The flow rate was set by adjusting the 15-centimeter- (6-in. -) diameter butterfly valve and placing porous resistance in the duct just upstream of the test section.

The duct was made to appear acoustically infinite in length by placing absorbing material both upstream and downstream of the test section. The pressure response of the duct was measured by flush, wall-mounted microphones.

### Flow Duct

The rectangular duct has a 3.81-centimeter by 10.16-centimeter ( $1\frac{1}{2}$ -in. by 4-in.) cross section (fig. 9). An exponential horn was attached to the upstream end of the test section. The horn can be removed if the experiment dictates. For these experiments the horn was filled with acoustic foam to approximate a  $\rho_0 c_0$  termination, which simulates an infinitely long duct.

The 1.4-meter- (4-ft, 8-in. -) long section just downstream of the horn is the actual test section. It consists of 16 detachable plates (8 on top and 8 on the bottom).

These plates are used to mount microphones, orifices, or pressure probes as the experiment dictates.

The next 1.8 meters (6 ft) of the duct contain an acoustic muffler made from two strips of acoustic foam (3.8 cm by 3.2 cm by 183 cm;  $1\frac{1}{2}$  in. by  $1\frac{1}{4}$  in. by 6 ft). These strips are mounted on a wooden support frame and inserted into the duct. The muffler serves two purposes: First, to attenuate any noise generated by the suction apparatus downstream of the test section; and second, to minimize the axial duct modes caused by reflection from the duct ends and by discontinuities of the duct. The muffler's transmission loss exceeds 40 decibels for frequencies above 1 kilohertz and 20 decibels for frequencies above 250 hertz.

Fixed to the end of the rectangular duct is a circular pipe that leads to the suction apparatus. As mentioned, the flow is controlled by two valves: A cutoff valve connects the apparatus to the main exhaust facility; a pneumatically operated butterfly valve modulates the mass flow rate.

The existing valves were designed to handle mean duct flows with Mach numbers of about 0.5. In these experiments the mass flow rate was set by the desired flow through the orifice, which corresponds to duct Mach numbers of about 0.01. Unfortunately, leaks in the butterfly valves (tolerable in high-mass-flow-rate experiments) produced excessive mass flow rates. To overcome this problem, we installed a flow resistor, a wire screen in front of which we placed blocks of acoustic foam, between the muffler and the test section. Since varying the number of foam blocks varied the flow resistance and lowered the pressure drop across the orifice, we achieved finer control of the jet velocity.

### Noise Source

Drawing air through a small orifice generates a turbulent jet, which will excite all the duct modes. Each duct mode will decay or be amplified depending on how it reacts with the duct. Therefore, the turbulent jet is ideal for studying the interaction of a noise source with the duct walls. In contrast, for example, an electrically driven speaker acts like an oscillating piston whose noise source is made up predominately of a plane pressure wave that will not react with the duct walls. Circular orifices were used to force the air to enter the duct as a round jet. Three orifices 0.64, 1.27, and 2.54 centimeters ( $1/4$ ,  $1/2$ , and 1 in.) in diameter were machined into a 0.32-centimeter- ( $1/8$ -in.-) thick plate (fig. 10(a)). The holes were countersunk to present a sharp edge to the incoming flow. This precaution was necessary because cylindrical holes with thickness-to-diameter ratios between  $1/2$  and 2 exhibit screech tones, which we want to avoid. In addition, a 1.27-centimeter- ( $1/2$ -in.-) diameter tube 1.5 meters (5 ft) long was fitted to a test plate (fig. 10(b)) to produce a different type of jet noise.

Both the orifice plates and the long tube were mounted on top of the duct so that the jet would enter perpendicular to the duct axis, as shown in figure 11. The thin-orifice jet is initially laminar; the long-tube jet is initially turbulent.

To allow the air to enter parallel to the duct axis, we replaced the exponential horn with a plate, shown in figure 12, that contained a 1.27-centimeter- (1/2-in. -) diameter orifice. Later, results from this configuration are compared with results from the configuration shown in figure 11.

In these experiments, the orifices were mounted in the test section so that the countersunk side faced the inside of the duct and thus presented a smooth surface to the incoming flow. Consequently, there were no mechanical variations at the entrance to influence sound generation.

### Flow Measurement

The system orifice plate shown in figure 8 has a 9.78-centimeter- (3.85-in. -) diameter hole. This plate was sized to measure flows with Mach numbers of about 0.5; consequently, it could not be used to measure the small flows encountered in these experiments. Instead, the pressure drop measured across the orifices through which the flow is drawn into the duct was used to estimate the jet velocities.

The orifice velocities were estimated from the atmospheric pressure and the static pressure just upstream of the exponential horn. Standard orifice equations (ref. 13, section 4-61) were used to calculate the orifice jet velocities for a discharge coefficient of 0.61 and an adiabatic process. These calculated velocities, which are presented later with the acoustic results, are only rough estimates of velocity, not exact values, since the flow streamlines and instrumentation do not match the standard orifice configuration.

As an additional cross-check, a hot-wire anemometer was used to measure the mass flow rate for both end- and side-oriented orifices (fig. 13). The square of the probe voltage is approximately proportional to the square root of the mass flow rate. The mass flow rate is predicted from the pressure drop across the orifice in the manner described. Each value of mass flow rate corresponds to a measured probe voltage. Since the flow rates for the side- and end-oriented orifices coincided, the flow rate apparently is not sensitive to orifice orientation. Consequently, the standard orifice equations probably give reasonable estimates of the flow rate.

### Microphone Procedure

In an experimental run, the pressure in the duct was reduced to below atmospheric.

Air then flowed through the orifice, hit the opposite wall (fig. 11), and flowed down the duct into the altitude header (fig. 8). The turbulent fluctuations generated by the orifice jet acted as an acoustic source.

These acoustic fluctuations were detected by a microphone at a certain minimum distance from the orifice. Two effects determine this minimum distance:

(1) Near the jet, in the mixing region, the turbulent fluctuations are strong enough to completely mask the acoustic fluctuations; therefore, the microphones must be outside this region. In these experiments, the microphone was upstream of the orifice near the exponential horn (fig. 9), where the mean flow is zero. Here, the convected turbulence is negligible. Data are presented later on to assess the effect of microphone placement (see section Effects of Microphone Location).

(2) The second consideration involves the detection of higher order acoustic modes. Although the frequency of a disturbance is below the mode cutoff frequency, the transverse pressure waves associated with the mode will exist near the source. These pressure waves, however, decay exponentially with distance. If the lowest mode is to be attenuated by a factor  $1/e$ , the microphone should be placed  $2b$  from the source,  $b$  being the width of the duct, where it will detect only propagating modes. For frequencies just below cutoff, the cutoff mode may be detected depending on how close the frequency is to the cutoff frequency.

In the experiments, two 0.64-centimeter- (1/4-in. -) diameter condenser microphones were used to determine the acoustic field. The response of these microphones was flat to 25 kilohertz. A standard acoustic source was used to check the system amplification. This source generated a 114-decibel signal in 5-octave steps from 0.125 to 2.0 kilohertz. The microphone was placed in the source and the resulting decibel level of the output was noted. In this way an absolute scale was established for the SPL. One microphone was mounted with its membrane flush with the surface of a test plate (protective shields were removed). A typical microphone position is shown in figure 14. In general, only one microphone was used for most tests, except in one experiment comparing up- and downstream radiation patterns.

One purpose of the present experiment was to detect the excitation of propagating higher order duct modes. Higher order acoustic modes are characterized by their pressure variations across the duct cross section. For it to detect these modes, the microphone must be at a pressure antinode, which in a rectangular duct is in a corner. Two plates were made with the microphones mounted in a corner. A third plate was machined to allow the transverse position of the microphone to vary (fig. 14). This plate had a double row of 0.64-centimeter- (1/4-in. -) diameter holes with 1.27-centimeter (1/2-in. ) separation between the centers. The second row was staggered behind the first to vary the microphone location by 0.64 centimeter (1/4 in. ). The holes were stopped with aluminum plugs when the microphone was not in place.

## Instrumentation

The measuring apparatus used in this study is shown in the block diagram of figure 15. The acoustic results were obtained from the x-y recorder, which recorded the output of the spectrum analyzer. Two frequency ranges were explored: 0 to 5.12 kilohertz and 0 to 25.6 kilohertz. Each range consisted of 256 frequency bands to provide bandwidths of 20 and 100 hertz, respectively. The temperature in the duct was assumed to be ambient.

The 0- to 5-kilohertz frequency range spans the first four higher order modes in the duct. In this range the frequency separation between modes is sufficient to reveal the excitation of the individual modes. In the 0- to 25-kilohertz range, however, the modal density  $\Delta N/\Delta k_0$ , defined by equation (19), increases with frequency. In this range, the spectrum analyzer will not be able to discern discrete pressure spikes at the higher cross-mode eigenfrequencies.

## Summary of General Procedure

In each experiment, an orifice was mounted in the test section, and then the flow-duct system valves were opened to reduce the pressure inside the duct. The flow rate through the orifice was set by inserting flow resistance in the duct as required and adjusting the butterfly valve. A microphone was placed in the far field of the source, and the instrumentation was activated to record the noise signal. The noise signal was Fourier analyzed, and separate averages of 256 channels were computed by the spectrum analyzer and plotted on the x-y recorder.

## DISCUSSION OF RESULTS

In this section, the experimental results are discussed in the following categories: basic effects and the effects of jet velocity, screech, Strouhal frequencies, inlet turbulence, duct resonances, axial orientation of orifice, microphone location, and mode shape.

### Basic Effects

In the basic experiment, a 1.27-centimeter- (1/2-in. -) thick orifice plate was mounted in the test section as shown in figure 9, and air was drawn through it into the duct. The turbulent fluctuations thus generated act as an acoustic source. The result-

ing acoustic pressure oscillations travel through the duct and are detected by the microphone system. The noise spectra associated with these oscillations are shown in figure 16.

Recall from earlier theoretical discussions that the influence of modes on the acoustic spectrum is most evident at low frequencies, when the separation between modes is large and the number of propagating modes small (fig. 7). At high frequencies the effect of an individual mode is averaged out; hence the spectrum tends toward that of a jet in free space. In the 0- to 5-kilohertz range, the SPL increases abruptly near the mode cutoff frequency (fig. 16(a)). The effect is quite pronounced in the first three modes. In the 0- to 25-kilohertz range, the acoustic spectrum changes character (fig. 16(b)). Above 7 kilohertz, pressure spikes are no longer clearly evident at the eigenfrequencies. Pressure spikes of neighboring modes overlap and minimize the influence of any single mode. The modal density eventually becomes too great for the 256-channel spectrum analyzer to separate the individual pressure spikes; consequently, the spectrum represents an average of many modes. To this extent, the SPL spectrum above 7 kilohertz (fig. 16(b)) is roughly comparable to the SPL spectrum of a jet exhausted into free space, which confirms the theory.

Thus, the basic experiment had the anticipated results.

#### Effects of Jet Velocity

To determine the effect of jet velocity on the acoustic spectrum, we chose several pressure drops across the orifice. Representative acoustic spectra over a range of jet velocities are presented in figure 17 for the 0.64-, 1.27-, and 2.54-centimeter- (1/4-, 1/2-, and 1-in. -) diameter orifices mounted on the side of the plate as shown in the sketch in figure 17(a).

The spectra for the 0- to 5-kilohertz range (fig. 17) reveal pressure spikes at each mode eigenfrequency (see also fig. 16). These asymmetric pressure spikes persist throughout the range of orifice diameters and Mach numbers tested. However, the overall acoustic level rises as the Mach number is increased. Moreover, the spectral intensity shifts to the higher modes as the mean velocity is increased, which is shown by the magnitudes of the first and fourth modes in figures 17(a) and (c) for increasing Mach number. Figure 17(b), however, does not follow this trend, particularly at Mach 0.44. The SPL of these fluctuations increases with increasing velocity. Thus, for a source of this type, there is generally an increase in level with velocity as well as a shift in level to higher frequencies.

The spectra in the 0- to 25-kilohertz range (fig. 18) are relatively smooth, like a free-jet spectrum, above 5 kilohertz. In figures 18(a) and (b), dashed lines representing the average behavior of the spectra are drawn through the highest velocity

curves. In figure 18, the peak Strouhal number is about 0.2, which is like that of a free jet (ref. 4).

### Effects of Screech

Screech peaks occur at the higher Mach numbers in figure 18. These peaks are not caused by the action of the duct walls on the jet noise source. If they were, the curve would resemble that for low-frequency oscillation - a discontinuous jump at a cutoff frequency and a slow decay in level above the cutoff frequency. Since the screech peaks are symmetric about their maximum, there is probably a different cause. Screech is generally considered a nonlinear process in which the acoustic field can react back on the jet. Under this condition, intense pure-tone oscillations that are caused by a jet impinging on a plate can be detected (ref. 14, ch. 4).

Similar symmetric noise peaks also occur, for example, when air flows over resonator cavities (refs. 15 and 16). The shedding of vortices by the flow over the resonator cavity holes coupled with the cavity resonance or even the duct mode resonance (ref. 15) produces these symmetric noise peaks. For screech and cavity-induced noise, the simple source model does not adequately describe the feedback mechanism.

### Effect of Equal Peak Strouhal Frequencies

The average shape of the spectrum is dominated by the location of the peak frequency. The distribution in acoustic intensity with frequency should be similar for different orifices with approximately equal peak Strouhal frequencies. However, the absolute value of the intensity will be higher for the larger diameter orifice with the higher jet velocity, as shown in figure 19 for three orifice diameters and three Strouhal frequencies.

To look in more detail at the rise in overall acoustic level with increasing velocity and diameter, we assumed that the radiative power in the duct is proportional to  $v^8 D^2$  (ref. 6, p. 93), as for free jets. If the spectrum shapes are identical, the power per unit frequency should also increase. The acoustic level ratio between orifices of different diameters but similar Strouhal frequencies is

$$\Delta\text{SPL} = 10 \log \frac{v_1^8 D_1^2}{v_0^8 D_0^2}$$

or

$$\Delta\text{SPL} = 80 \log \frac{v_1}{v_0} + 20 \log \frac{D_1}{D_0}$$

For equal Strouhal numbers,  $(\nu D_0/v_0)$  equals  $(\nu D_1/v_1)$ ; therefore, if the orifice diameter is doubled, as in figure 19, the velocity must double to keep the peak Strouhal number constant; thus

$$\frac{D_1}{D_0} = \frac{v_1}{v_0} = 2$$

and

$$\Delta\text{SPL} = 80 \log 2 + 20 \log 2 = 30 \text{ dB}$$

The difference in level of both spectra in figure 19 is approximately 30 decibels, as predicted.

Although this result holds for high-frequency spectra, where the duct response is similar to the free-space response, it is only approximate for low-frequency spectra. One noteworthy exception is the behavior of the spectra below the first cutoff frequency. This behavior is most pronounced in figure 19(c) below 2.0 kilohertz, where the spectrum for the 0.64-centimeter- (1/4-in. -) diameter orifice with the lower Mach number decays from  $\nu = 0$  to the SPL pressure spike at the first cutoff frequency. However, the spectrum for the 1.27-centimeter- (1/2-in. -) diameter orifices with the higher Mach number does not decay. (Note that the low-frequency spectra of fig. 17 also decay with frequency at low Mach numbers.)

At low Mach numbers the behavior below the first mode may be dominated by the sound resulting from the complex recirculation patterns along the wall (fig. 11) rather than by the orifice jet noise, as shown by the schematic in figure 20. That is, as the level of the jet spectrum is decreased, the recirculation noise source could be uncovered, which could account for the dip in the SPL spectrum before first-mode cut-on. The spectrum shape below the first cutoff will, of course, depend on the relative strengths of the various duct noise sources.

#### Effect of Inlet Turbulence

If the pressure spikes in the 0- to 5-kilohertz frequency range are due solely to

the duct's response to a turbulent jet source, changes in inlet turbulence should not obscure this effect. To test this thought, we altered the turbulent nature of the inlet jet flow. The flow entering the duct from a square-edge orifice is laminar; it becomes turbulent further downstream. The flow entering the duct from a long tube, on the other hand, is fully turbulent. If the duct's response depends only on the turbulent jet sources, the change in the jet flow from laminar to turbulent near the tube outlet should not destroy the effect. These considerations were checked by allowing the flow to enter from a 1.5-meter- (5-ft-) long tube of 1.27-centimeter (1/2-in.) inside diameter mounted on the side of the duct (fig. 12).

The acoustic spectra in the 0- to 5-kilohertz range (fig. 21(a)) still contain discrete pressure spikes at the cross-mode frequencies. Thus, the initial turbulence level of the jet core probably has a very small effect on the turbulent shearing region. The acoustic spectra in the 0- to 25-kilohertz range (fig. 21(b)) again resemble the free-space spectra at high frequencies. A peak in level occurs at approximately the peak Strouhal number of 0.2, which is consistent with previous behavior. Screech peaks are absent from these curves; however, the velocity range explored is not sufficient to resolve the influence of inlet turbulence on screech. Screech has been observed in turbulent jets (ref. 14, section 4.3.5).

#### Effect of Duct Resonances

Periodic oscillations in amplitude with frequency resulting from resonance in the long tube appear in figure 21(a). Acoustically, the inlet tube acts like open organ pipes, for which the resonant frequencies are given by

$$\nu_n = \frac{c_0 n}{2L} (1 - M_p^2) \quad (20)$$

where the wavelength of the sound must be larger than the tube diameter, and the inductive end correction is neglected. The symbol  $M_p$  represents the average flow Mach number in the tube. The difference in frequency between two adjacent resonances of the pipe is

$$\Delta\nu = \nu_{n+1} - \nu_n = \frac{c_0}{2L} (1 - M_p^2) \quad (21)$$

For a 1.5-meter- (5-ft-) long pipe with Mach 0.2 flow,  $\Delta\nu$  is 108 hertz, which is close to the measured spacing between peaks of 112 hertz. Therefore, the ripples in ampli-

tude with frequency in figure 21(a) represent the excitation of the axial pipe modes that are superimposed on the duct's acoustic response. The peaks in the ripples represent the axial resonance condition in the pipe.

Similarly, axial (z-direction) acoustic modes can be excited by sound-wave reflections at the ends of the flow duct. In the study of reference 17, symmetric pressure oscillations were induced in a fan inlet by varying the inlet length to induce axial resonance. In the present study, axial resonances were minimized by the entrance muffler and the foam-filled exponential horn (fig. 9).

### Effect of Axial Orientation of Orifice

The position of the orifice was altered so that the jet entered the duct parallel to the duct axis: The exponential horn was removed from the upstream end and a 1.27-centimeter- (1/2-in. -) thick orifice plate was inserted in its place (fig. 13). The duct then resembled a semi-infinite duct with a hard-wall entrance, rather than the infinite duct developed in the theory.

Acoustic spectra in the 0- to 5-kilohertz range as a function of Mach number (fig. 22) again show the basic effects of discrete level changes at the cross-mode eigenfrequencies. The noise levels for side- and axially oriented holes are about the same (see also fig. 17(b)). However, the considerably higher low-frequency noise for the axial jet tends to obscure the first peak. Because of this and because the side-oriented orifice gave results more nearly matching theory, we chose to use side-oriented orifices.

### Effects of Microphone Location

Except for experiments with the axially oriented orifice, all experiments were performed with the microphone located upstream. In the upstream region, there is no convected turbulence to mask the acoustic fluctuations. In addition, there is no change in duct response with jet velocity, because there is no mean flow upstream of the orifice. However, since the mean flow downstream of the orifice is low, there should be no pronounced differences in the upstream and downstream radiation.

To test the effects of microphone location, we used two microphones: one upstream and one downstream of a side-oriented orifice. The acoustic spectra from the two microphones were then plotted on the same graph for jet Mach numbers of 1.00 and 0.25 (fig. 23). At Mach 0.25 the responses of the upstream and downstream microphones differed by only 0.8 decibel. At Mach 1.00 the difference was greater: The downstream spectrum varied periodically in level with frequency. And, though the downstream

spectrum was, on the average, identical to the upstream spectrum, it somewhat obscured the duct's response to a turbulent source. To avoid this, we placed the microphone upstream in all other experiments.

Another test was run while a second microphone was traversed axially along the centerline of the duct. As shown in figure 24, the position of the traversing microphone changes the SPL level detected by the stationary wall microphone and thus changes the standing wave pattern in the duct. Reflections from the traversing microphone dominate the duct response, most likely because of the relatively small duct cross-sectional area. Thus, inserting any probe into the flow duct of this facility may significantly alter the duct acoustics.

### Effect of Mode Shape

These experiments are intended to show conclusively that the duct response is due to the excitation of the higher order modes and to emphasize that the microphone must be placed at a pressure antinode. Therefore, the pressure level in the x-direction (fig. 1) was measured at three cross-mode eigenfrequencies:

Frequency, kHz	Number of propagating modes	Propagating modes
1	1	(0, 0)
1.8	2	(0, 0), (1, 0)
3.5	3	(0, 0), (1, 0), (2, 0)

As the frequency is increased above the mode cutoff frequency, the previously excited modes still propagate. However, slightly above the mode cutoff frequency, the duct response is dominated by transverse (x-direction in this case) variations of that resonant mode. The reason is the pole in the duct response (eq. (10)) at the cutoff frequency.

The measured SPL variations of the (0, 0), (1, 0), and (2, 0) modes shown in figure 25 correspond to the theoretical variations shown in figure 4. At 1 kilohertz, only the plane wave propagates and pressure does not vary across the duct cross section. At 1.8 kilohertz, the first asymmetric mode dominates the response - note the node at the center. At 3.5 kilohertz, the first symmetric mode dominates the response - note the antinode at the center.

The pressure fields in the various modes are additive. If a microphone is placed at

a pressure node for a given mode, the mode will no longer be detected. For the first asymmetric mode, we compared the acoustic spectrum at centerline to that at the corner (fig. 26). Because the center microphone position is a node for this mode, the peak was not detected.

## CONCLUSIONS

The following conclusions have been reached about a turbulent noise source in a rectangular duct:

1. In the frequency range 0 to 5 kilohertz, which includes only the first few duct modes, the duct walls have a strong influence on the acoustic spectra. The discrete nature of the first few higher order modes manifests itself in an asymmetric singularity (pressure spike) near the mode cutoff frequency.
2. In the frequency range 0 to 25 kilohertz, where the number of propagating modes is large and the intervals between modes are small, the influence of the duct walls is minimal and the acoustic spectrum is nearly as smooth as if the jet were in free space.
3. The asymmetric pressure spikes in a duct occur over a range of jet velocities, jet orientations, and inlet turbulence levels.
4. The qualitative structure of the frequency spectra can be interpreted through a linear analysis of the duct's acoustical response.
5. For enclosed jets, the intensity level appears to be proportional to  $v^8 D^2$ , where  $v$  is velocity and  $D$  is orifice diameter. That is, the relationships for free jets apply equally well to enclosed jets, for the limited data taken.

Lewis Research Center,  
National Aeronautics and Space Administration,  
Cleveland, Ohio, February 24, 1978,  
505-03.

## REFERENCES

1. Emmerling, J. J.; and Bekofske, K. L.: Experimental Clean Combustor Program, Noise Measurement Addendum, Phase 2. (R75AEG147-13-ADD, General Electric Co.; NASA Contract NAS3-18551.) NASA CR-135045, 1976.
2. Sofrin, T. G.; and Riloff, N., Jr.: Experimental Clean Combustor Program - Noise Study. (PWA-5458, Pratt and Whitney Aircraft; NASA Contract NAS3-18544. NASA CR-135106, 1976.

3. Ribner, H. S.: The Generation of Sound by Turbulent Jets. *Advances in Applied Mechanics*, vol. 8, H. L. Dryden and T. Von Karman, eds., Academic Press, 1964, pp. 103-182.
4. Olsen, W. A.; Miles, J. H.; and Dorsch, R. G.: Noise Generated by Impingement of a Jet Upon a Large Flat Board. NASA TN D-7075, 1972.
5. Lighthill, M. J.: On Sound Generated Aerodynamically, I. General Theory. *Proc. Roy. Soc. (London)*, Ser. A, vol. 211, no. 1107, Mar. 20, 1952, pp. 564-587.
6. Goldstein, Marvin E.: *Aeroacoustics*. NASA SP-346, 1974.
7. Ribner, H. S.: New Theory of Jet Noise Generation, Directionality and Spectra. *J. Acoust. Soc. Am.*, vol. 31, no. 2, Feb. 1959, pp. 245-246.
8. Morse, Phillip McCord; and Ingard, K. Uno: *Theoretical Acoustics*. McGraw-Hill Book Co., Inc., 1968.
9. Doak, P. E.: Excitation, Transmission and Radiation of Sound from Source Distributions in Hard-Walled Ducts of Finite Length. (I): The Effects of Duct Cross-Section Geometry and Source Distribution Space-Time Pattern. *J. Sound Vib.*, vol. 31, no. 1, Nov. 8, 1973, pp. 1-72.
10. Plumblee, H. E.; and Dean, P. D.: Sound Measurements within and in the Radiated Field of an Annular Duct with Flow. *J. Sound Vib.*, vol. 28, no. 4, June 1973, pp. 715-735.
11. Powell, Alan: How Does Fluid Flow Generate Sound? *Advances in Engineering Science*. NASA CP-2001 (vol. 3), 1976, p. 819.
12. Roberts, D. W.; and Johnston, J. P.: Development of a New Internal Flow Aeroacoustic Facility. SU-PD-18, Stanford Univ., 1974.
13. Marks, Lionel Simeon: *Mechanical Engineers Handbook*. Sixth ed., McGraw-Hill Book Co., Inc., 1958, section 4-61.
14. Succi, George Peter: The Interaction of Sound with Turbulent Flow. Ph.D. Thesis, Massachusetts Institute of Technology, 1977.
15. Bauer, A. B.; and Chapkis, R. L.: Noise Generated by Boundary Layer Interaction with Perforated Acoustic Liners. AIAA Paper 76-41, Jan. 1976.
16. Tsui, C. Y.; and Flandro, G. A.: Self-Induced Sound Generation by Flow over Perforated Duct Liners. *J. Sound Vib.*, vol. 50, no. 3, Feb. 8, 1977, pp. 315-331.
17. Baade, P. K.: Effects of Acoustic Loading on Axial Flow Fan Noise Generation. *Noise Contr. Eng.*, vol. 8, Jan.-Feb. 1977, pp. 5-15.

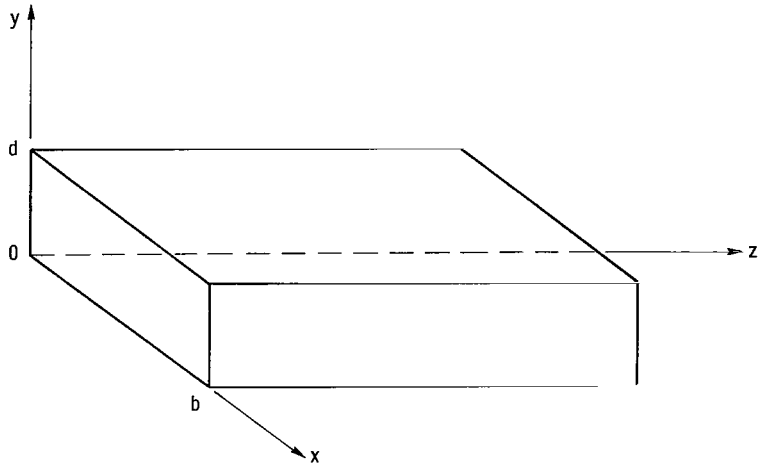


Figure 1. - Duct coordinate system.

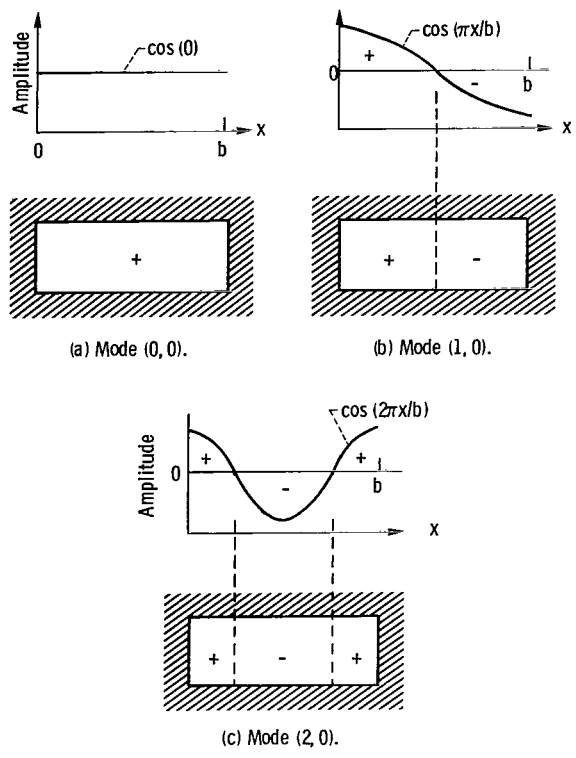


Figure 2. - Mode concept - spatial variation in pressure.

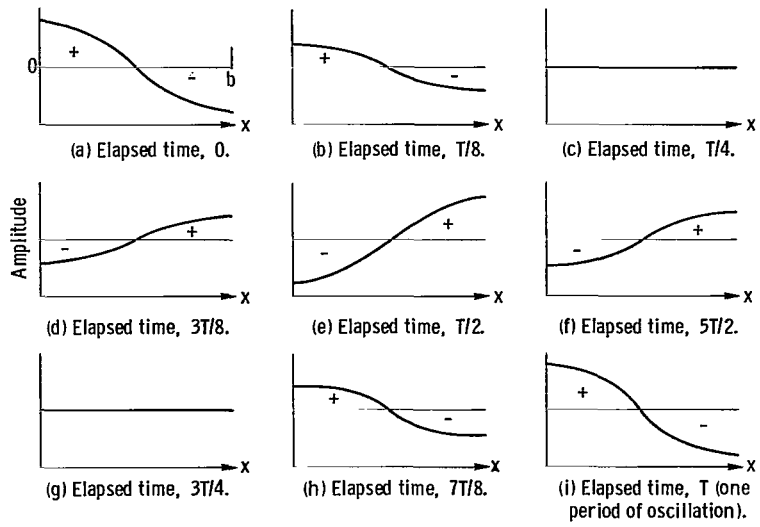


Figure 3. - Time dependency of spatial pressure variation for (1, 0) mode.

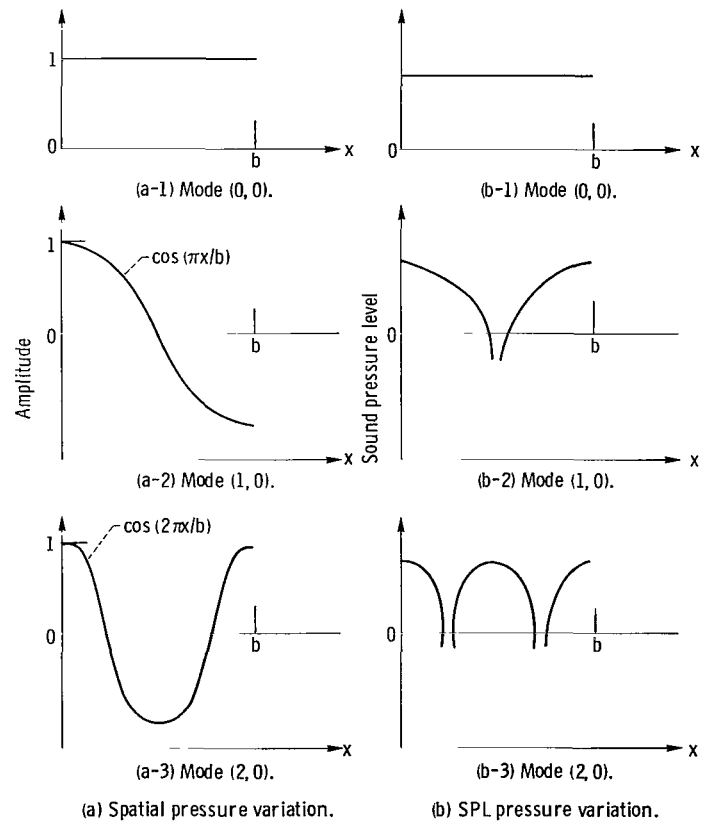


Figure 4. - Spatial pressure and sound pressure level (SPL) variations for modes (0, 0), (1, 0), and (2, 0).

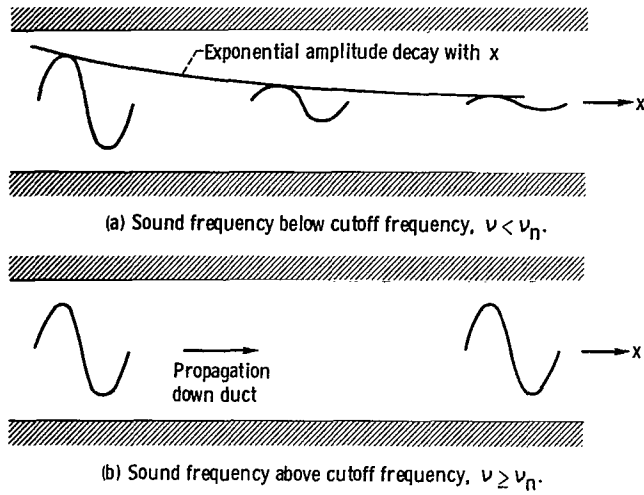


Figure 5. - Illustration of decaying and propagating modes, where  $\nu$  is mode oscillation frequency and  $\nu_n$  is cutoff frequency (predicted by theory).

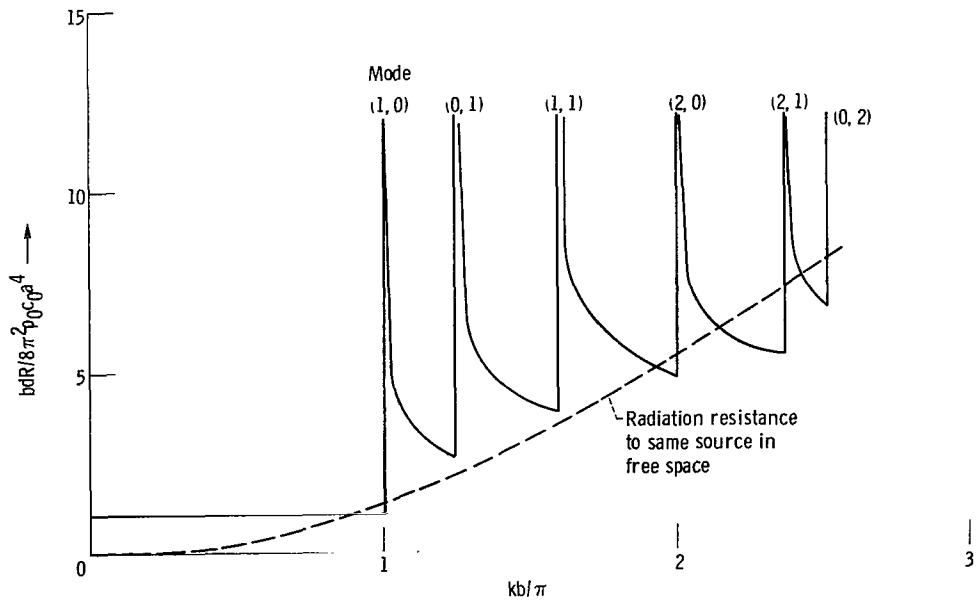
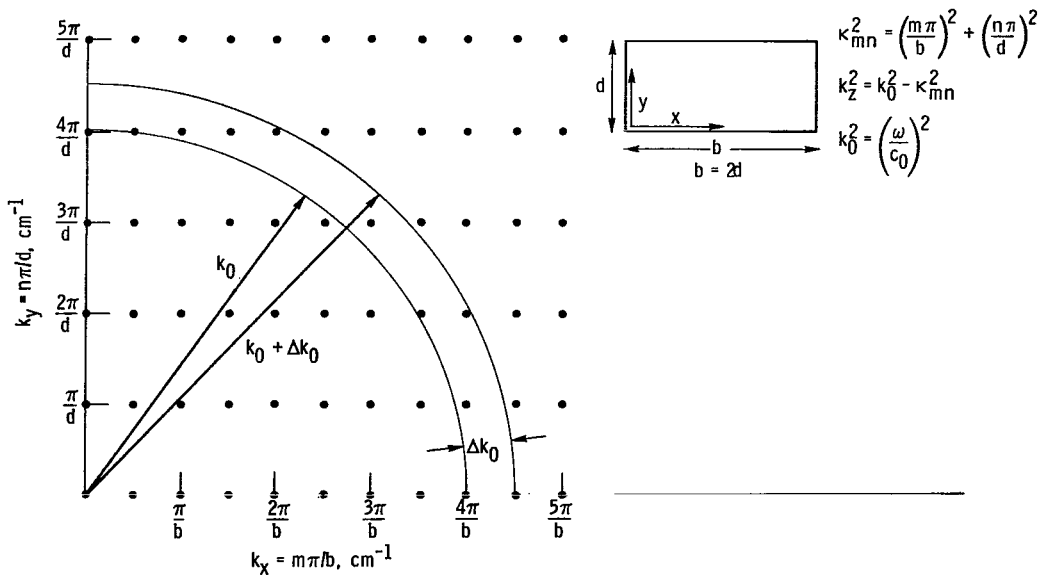
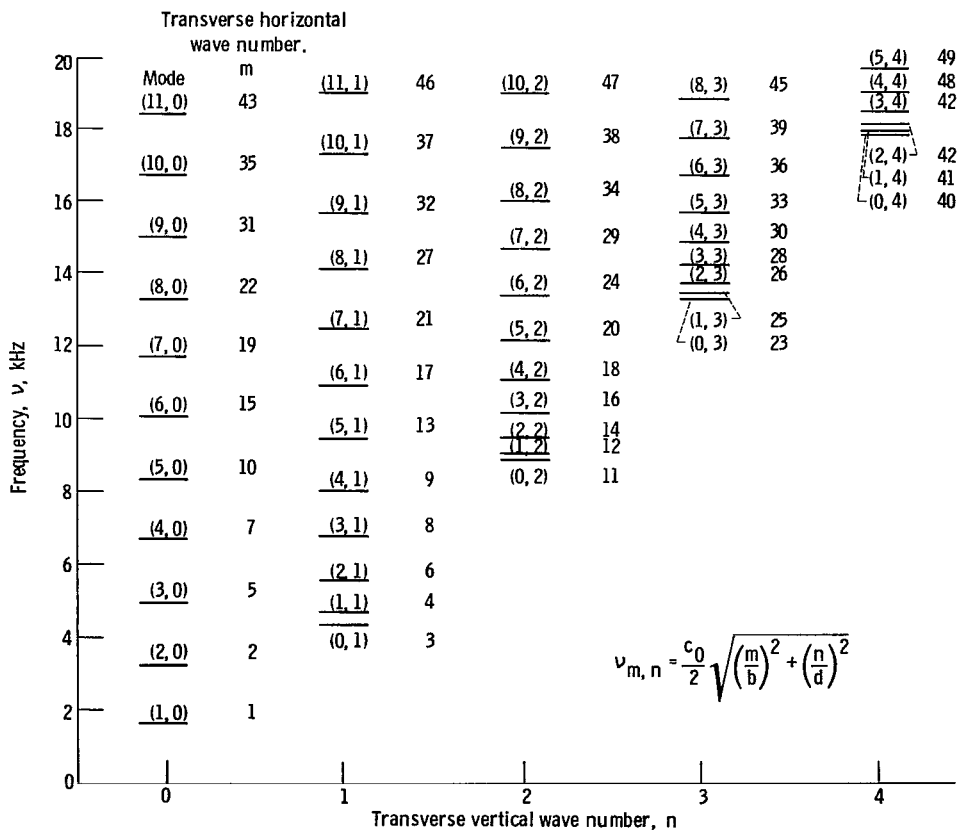


Figure 6. - Dimensionless radiative resistance  $R$  of a simple source of radius  $a$  at point  $(x_0, y_0)$  in a rectangular duct of sides  $b$  and  $d$ , where  $x_0 = 1/4 b$ ;  $y_0 = 1/10 d$ ; and  $d = 4/5 b$ . (From ref. 8.)



(a) Wave number graph for duct whose width is twice its height.



(b) Mode diagram for rectangular duct 3.81 cm (1.5 in.) high by 10.16 cm (4 in.) wide.

Figure 7. - Graphic illustration of mode cutoff.

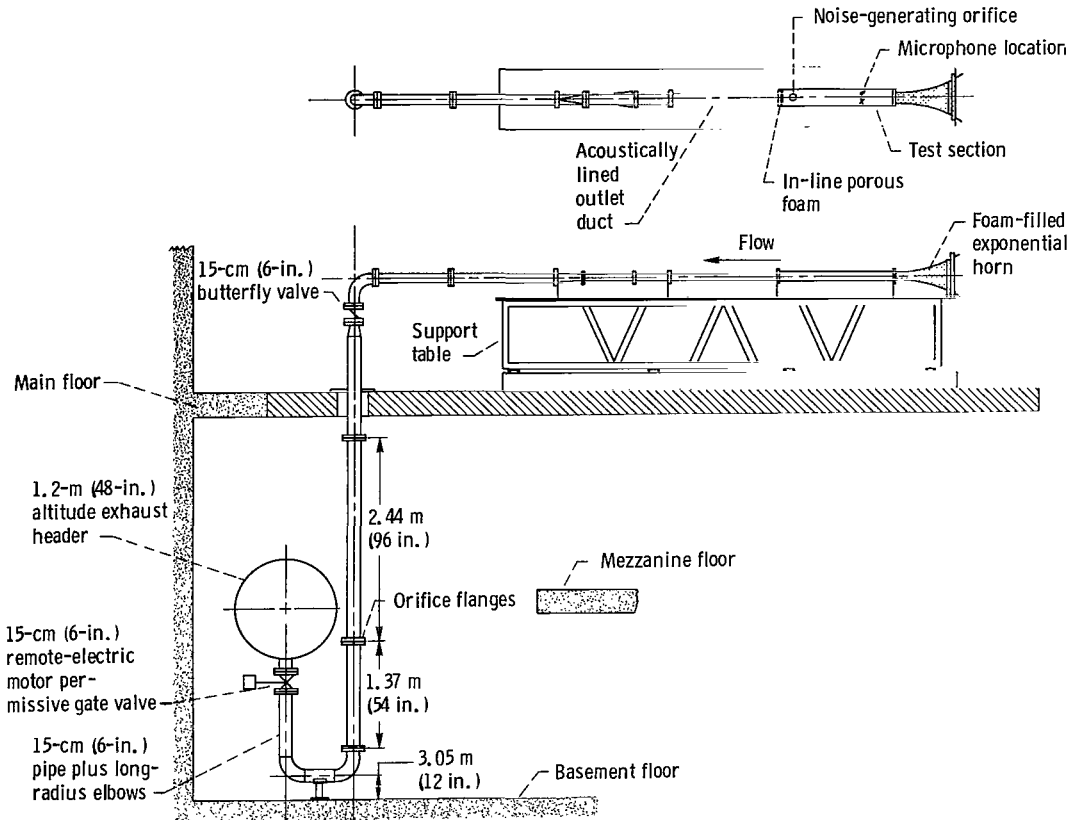


Figure 8. - Flow duct system.

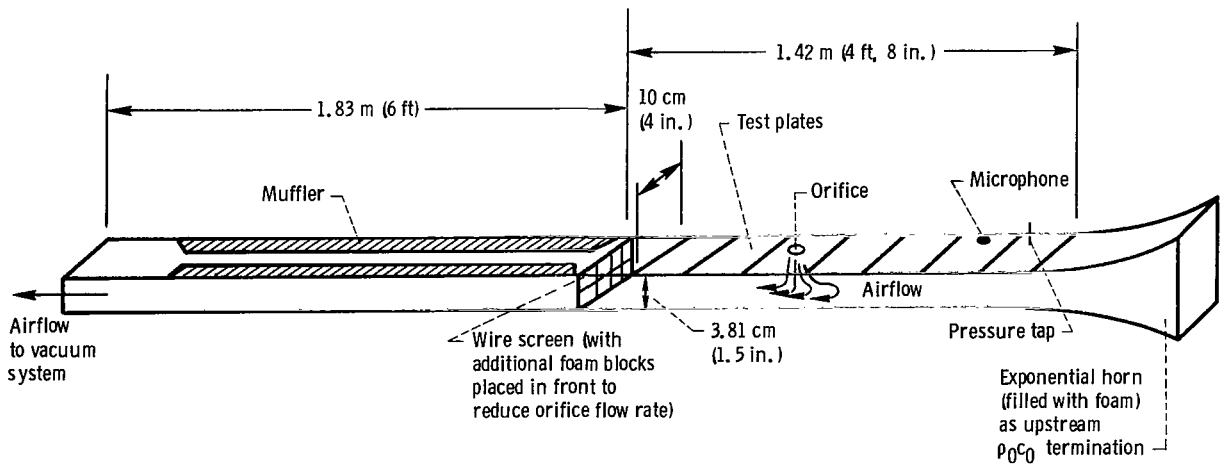
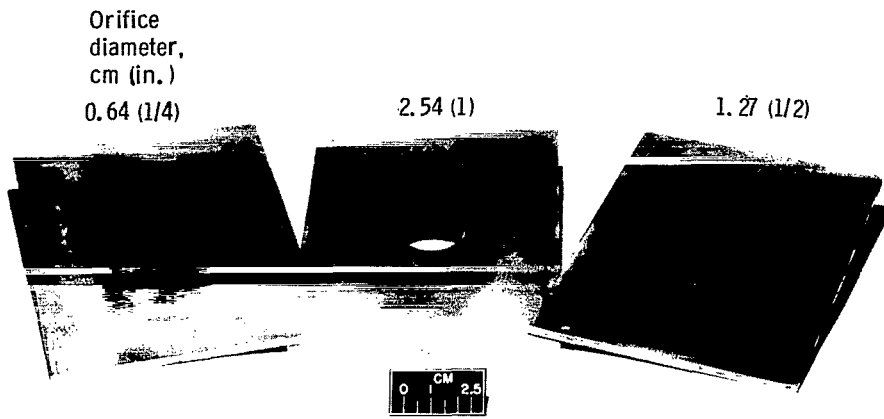
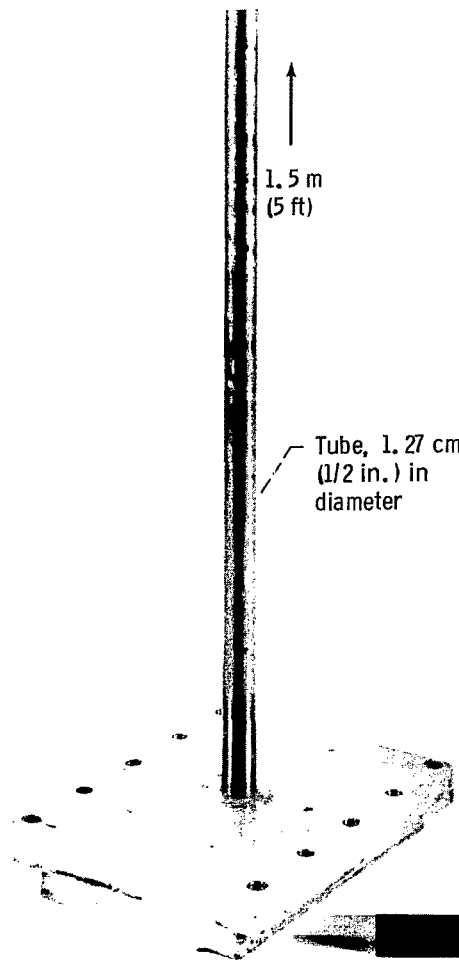


Figure 9. - Flow-duct test section.



(a) 0.32-Centimeter-thick plates.



(b) Long tube.

Figure 10. - Orifice plates.

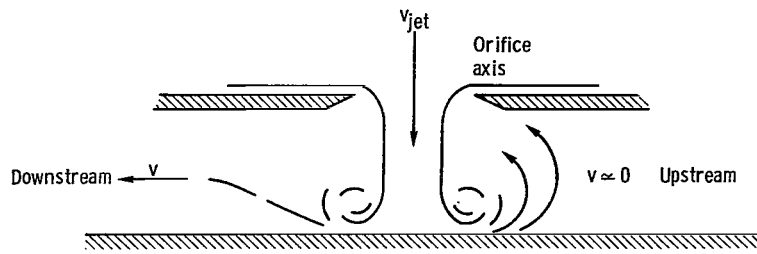


Figure 11. - Flow pattern of jet into duct.

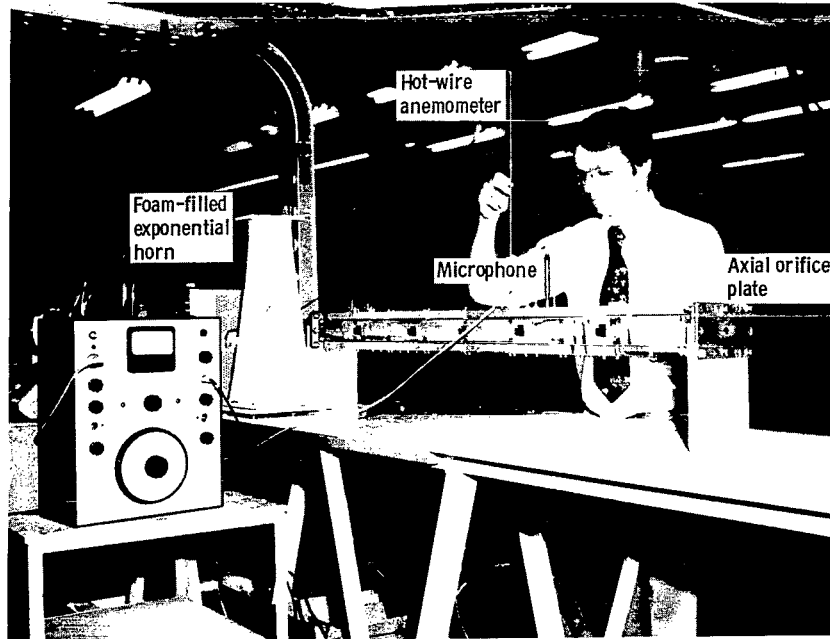


Figure 12. - Flow-duct apparatus.

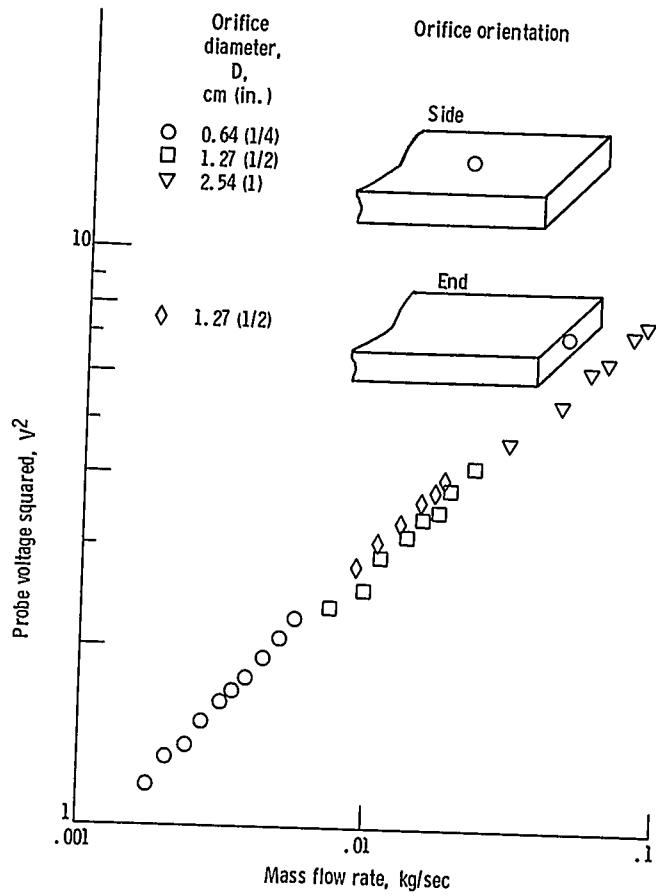


Figure 13. - Mass flow rate as measured by hot-wire anemometer.

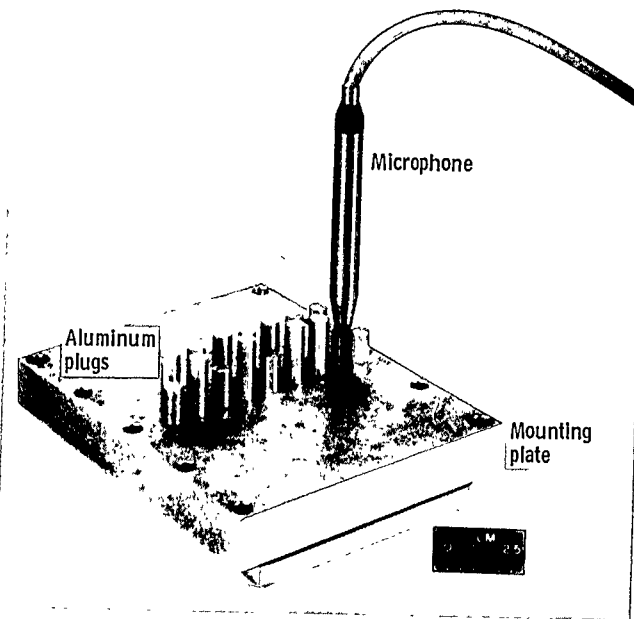


Figure 14. - Microphone positioning plate.

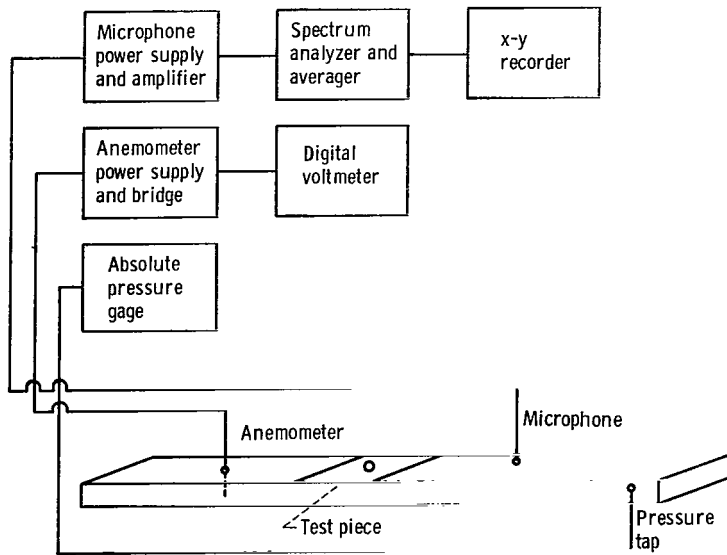
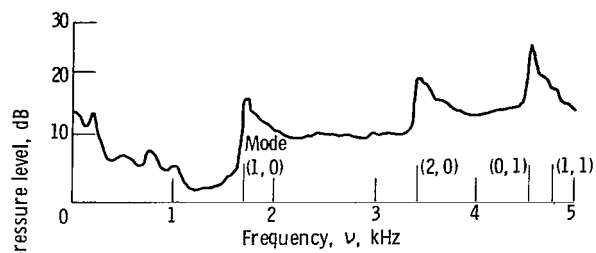
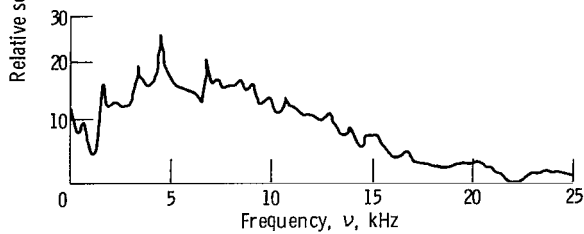


Figure 15. - Instrumentation.

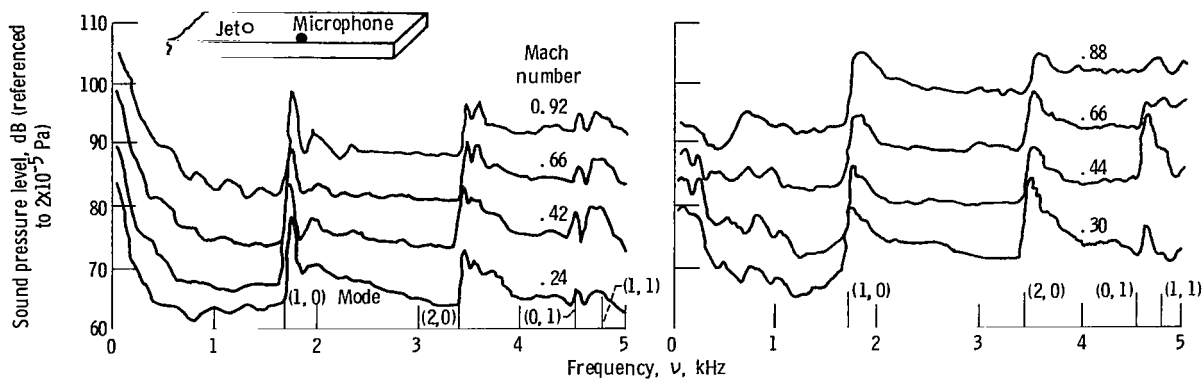


(a) Low-frequency range.



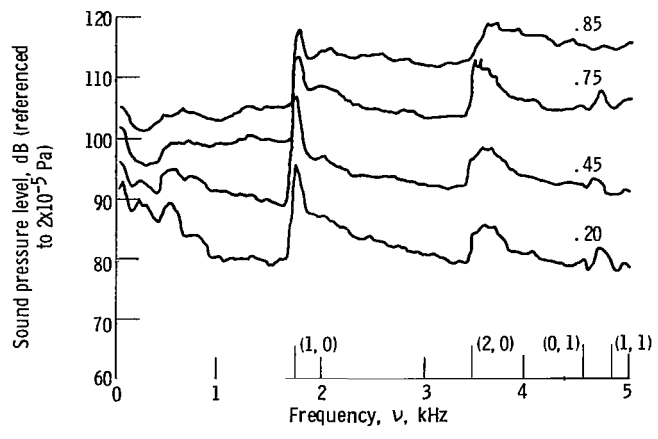
(b) High-frequency range.

Figure 16. - Low- and high-frequency spectra in a rectangular duct. Orifice diameter, 1.27 cm (1/2 in.); orifice orientation, top of duct; Mach number, 0.44.



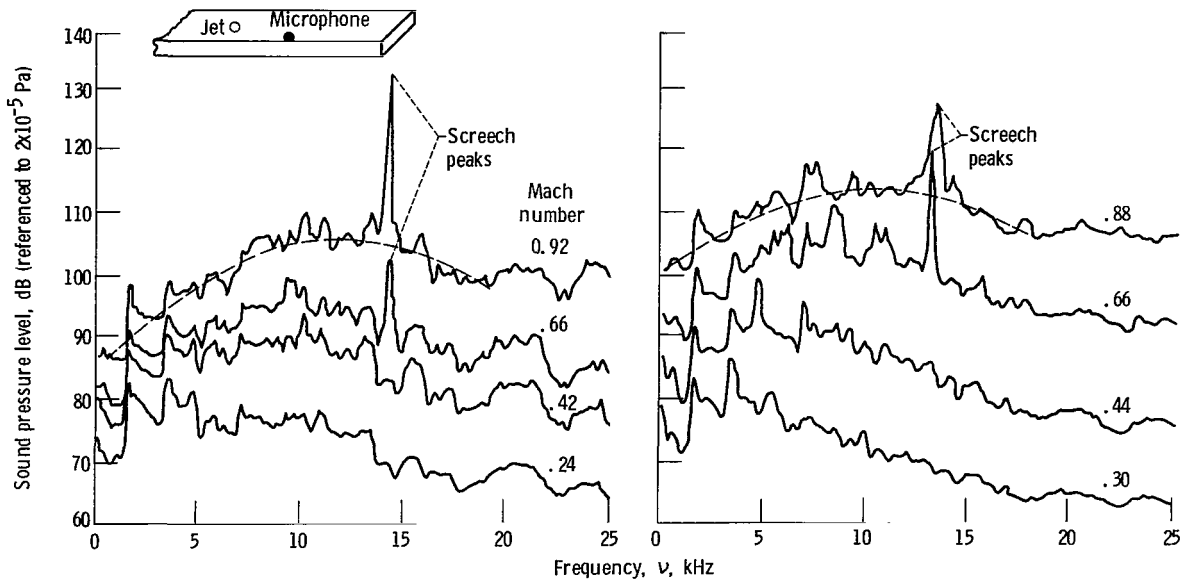
(a) Orifice diameter, D, 0.64 cm (1/4 in.).

(b) Orifice diameter, D, 1.27 cm (1/2 in.).



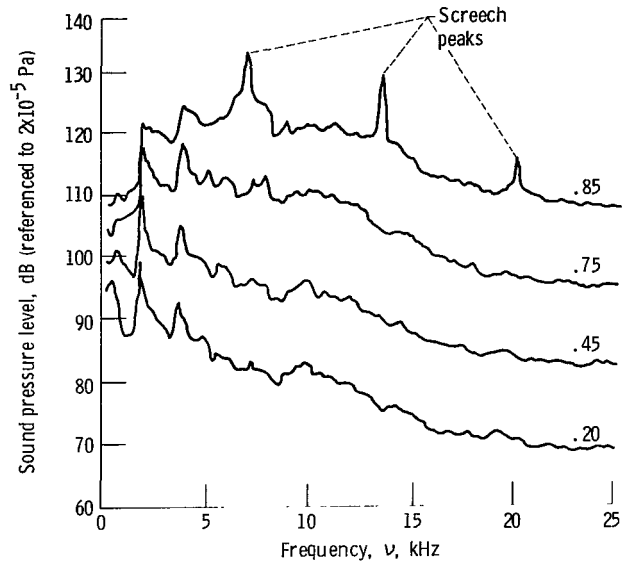
(c) Orifice diameter, D, 2.54 cm (1 in.).

Figure 17. - Effect of orifice jet velocity (Mach number) and orifice diameter on acoustic spectra in the low-frequency range (0 to 5 kHz).



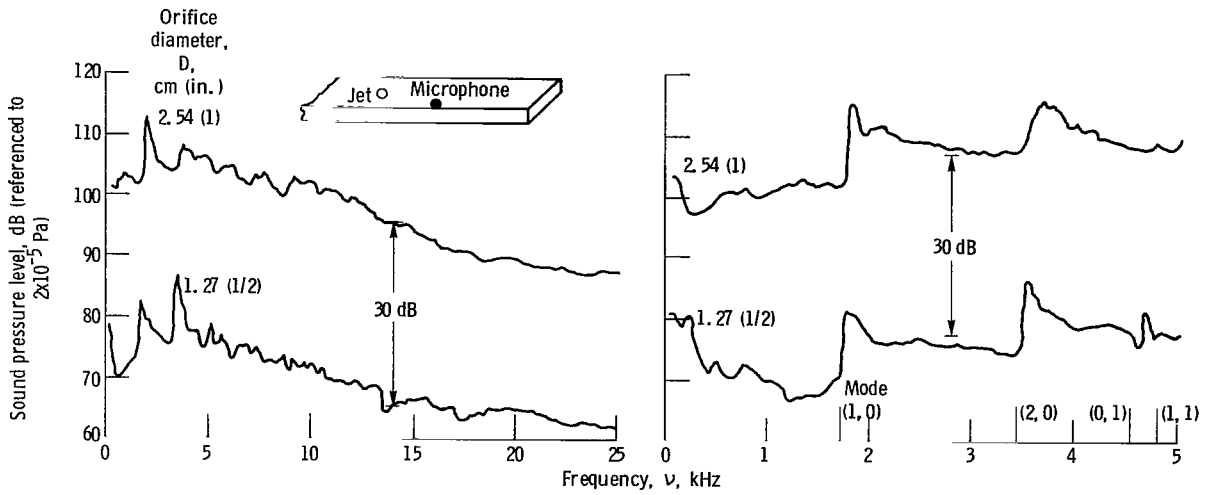
(a) Orifice diameter,  $D$ , 0.64 cm (1/4 in.).

(b) Orifice diameter,  $D$ , 1.27 cm (1/2 in.).



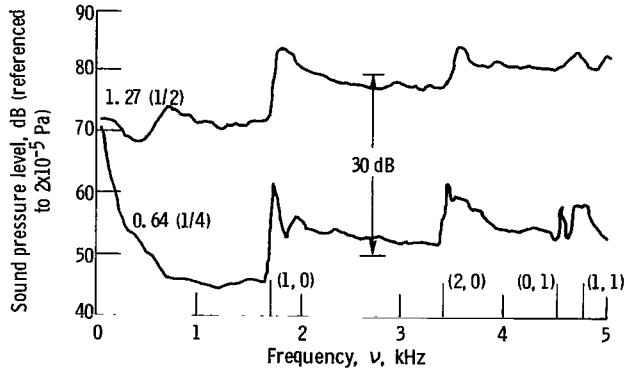
(c) Orifice diameter,  $D$ , 2.54 cm (1 in.).

Figure 18. - Effect of orifice jet velocity (Mach number) and orifice diameter on acoustic spectra in the high-frequency range (0 to 25 kHz).



(a) Strouhal frequency,  $\nu_s$ , ~1.9 kHz.

(b) Strouhal frequency,  $\nu_s$ , ~2.5 kHz.



(c) Strouhal frequency,  $\nu_s$ , ~5.7 kHz.

Figure 19. - Sound pressure levels for orifices with approximately equal peak Strouhal frequencies ( $\nu_s = 0.2 \nu/D$ ).

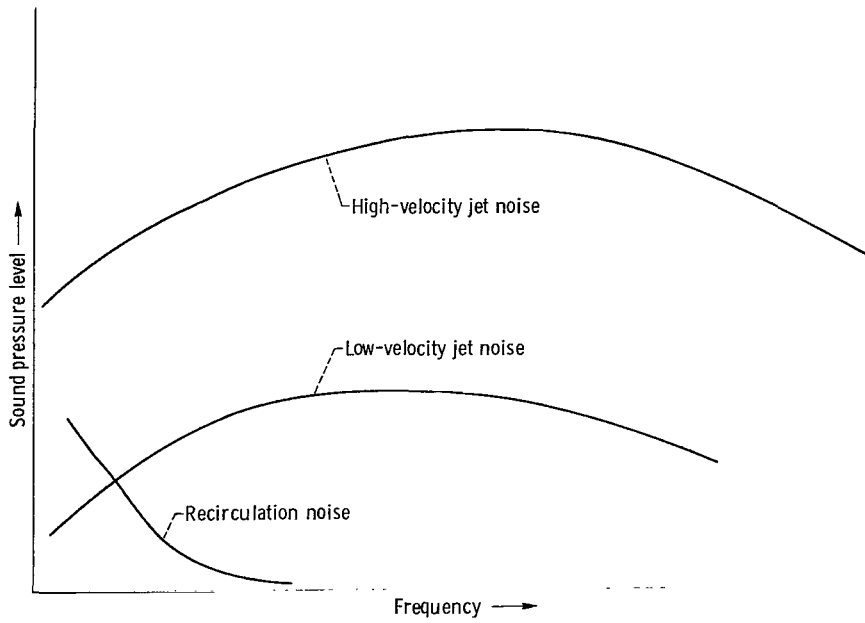


Figure 20. - Schematic representation of noise sources in flow duct.

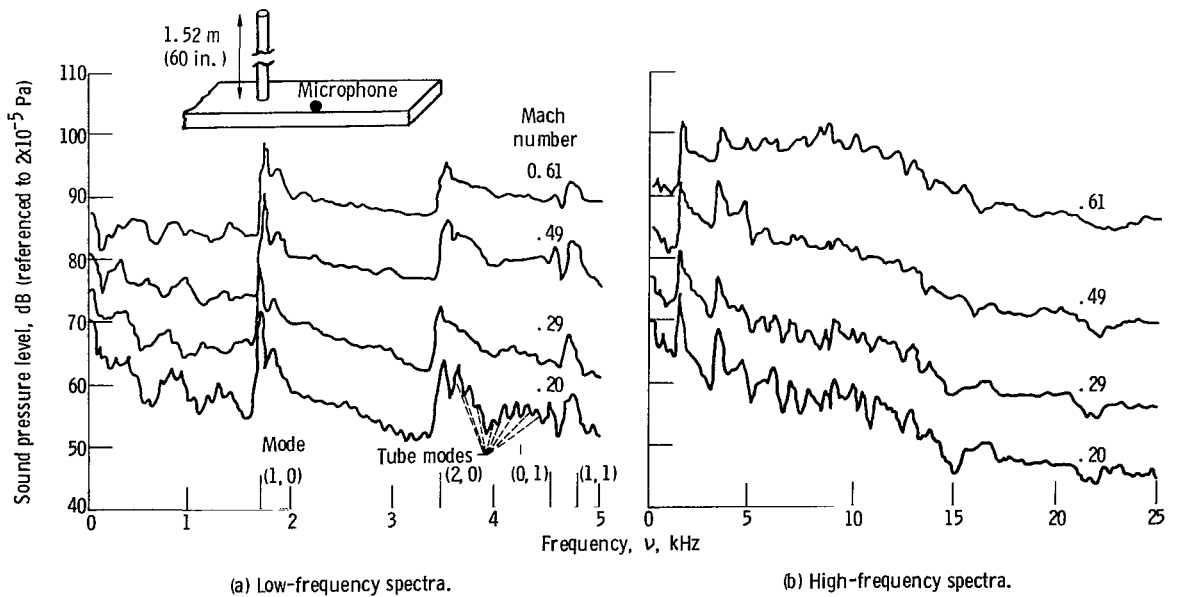


Figure 21. - Effect of velocity of flow entering orifice from long tube on acoustic spectra. Tube length, 1.52 m (60 in.); tube inside diameter, 1.27 cm (1/2 in.).

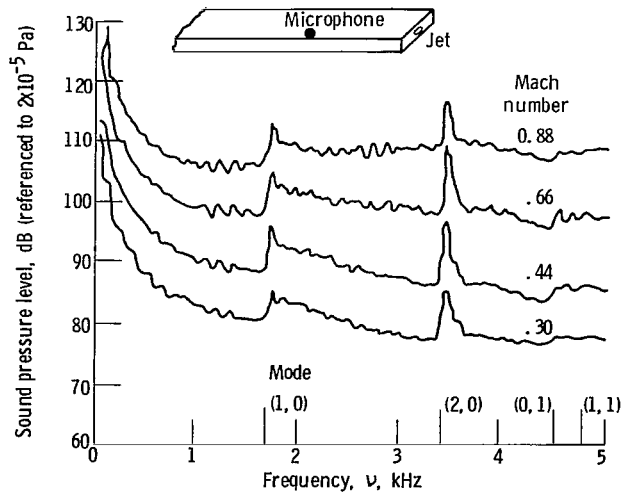


Figure 22. - Low-frequency spectra observed when jet and duct axis are parallel. Orifice diameter,  $D$ , 1.27 cm (1/2 in.).

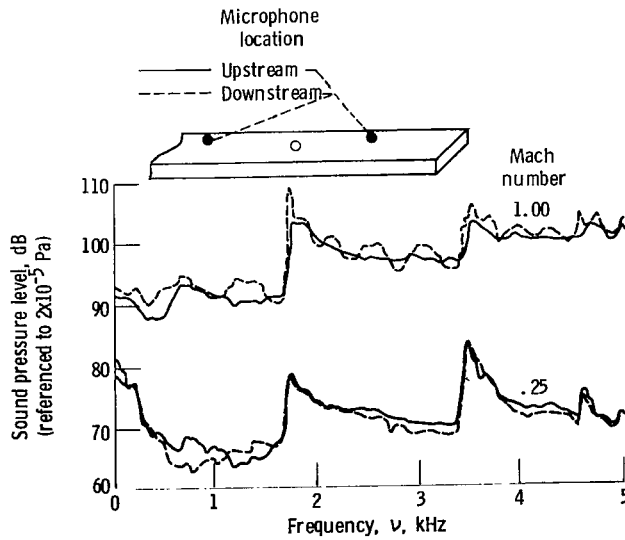


Figure 23. - Upstream- and downstream-radiated acoustic spectra.

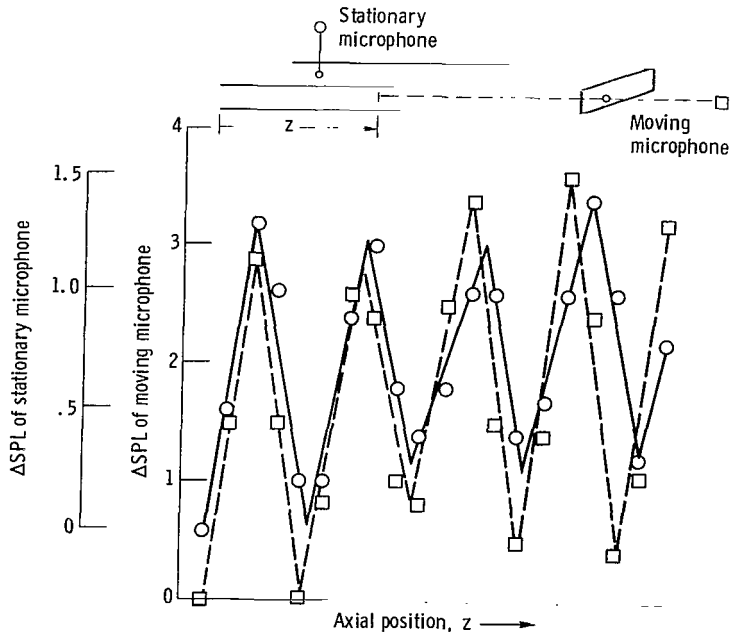


Figure 24. - Minimum-to-peak sound pressure level variations as function of microphone location.

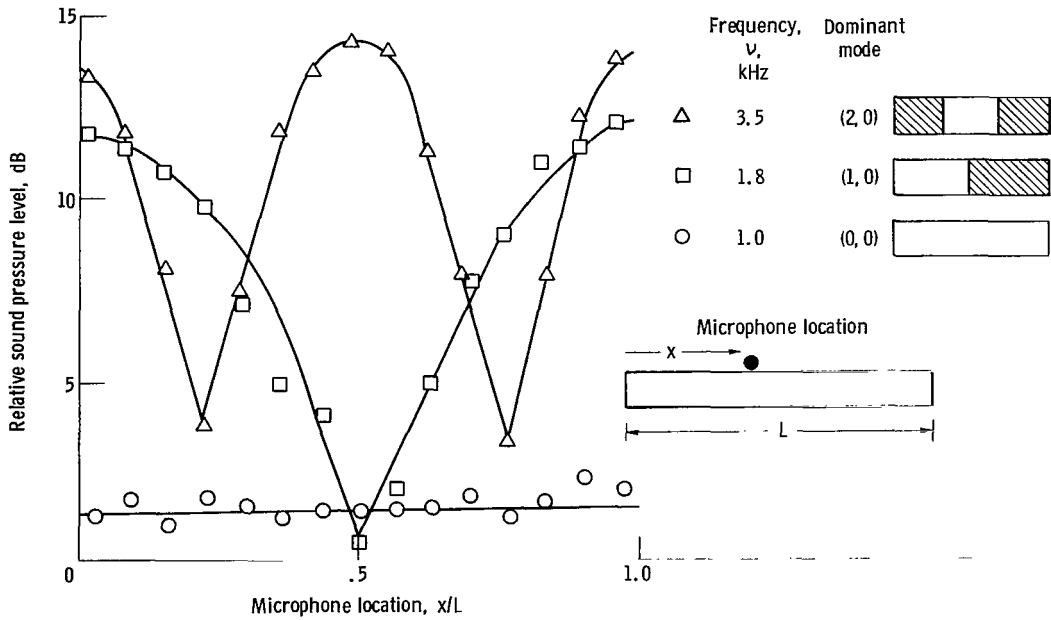


Figure 25. - Transverse variation of radiated sound levels at frequencies selected to show mode shape.

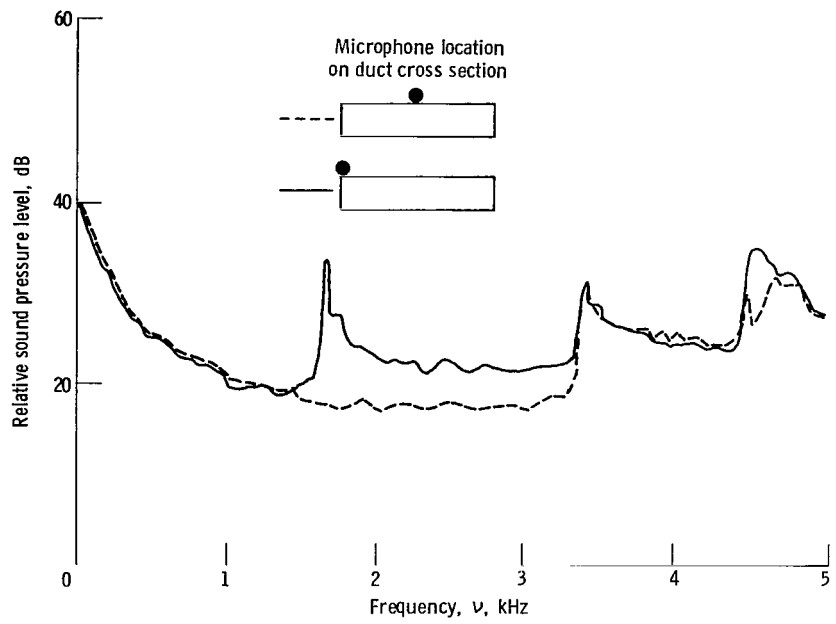


Figure 26. - Effect of microphone location on detected spectra.

1. Report No. NASA TP-1248		2. Government Accession No.		3. Recipient's Catalog No.	
4. Title and Subtitle <b>INTERACTION OF A TURBULENT-JET NOISE SOURCE WITH TRANSVERSE MODES IN A RECTANGULAR DUCT</b>				5. Report Date <b>June 1978</b>	
7. Author(s) <b>George P. Succi, Massachusetts Institute of Technology; Kenneth J. Baumeister, Lewis Research Center; and K. Uno Ingard, Massachusetts Institute of Technology</b>				6. Performing Organization Code	
9. Performing Organization Name and Address <b>National Aeronautics and Space Administration Lewis Research Center Cleveland, Ohio 44135</b>				8. Performing Organization Report No. <b>E-9462</b>	
12. Sponsoring Agency Name and Address <b>National Aeronautics and Space Administration Washington, D. C. 20546</b>				10. Work Unit No. <b>505-03</b>	
15. Supplementary Notes				11. Contract or Grant No.	
16. Abstract <p>A turbulent jet was used to excite transverse acoustic modes in a rectangular duct. The pressure spectrum showed asymmetric singularities (pressure spikes) at the resonant frequencies of the duct modes. This validates previously published theoretical results. These pressure spikes occurred over a range of jet velocities, orientations, and inlet turbulence levels. At the frequency of the spike, the measured transverse pressure shape matched the resonant mode shape.</p>				13. Type of Report and Period Covered <b>Technical Paper</b>	
17. Key Words (Suggested by Author(s)) <b>Noise; Turbulent; Jet; Duct; Modes; Singularities</b>				14. Sponsoring Agency Code	
18. Distribution Statement <b>Unclassified - unlimited STAR Category 01</b>					
19. Security Classif. (of this report) <b>Unclassified</b>		20. Security Classif. (of this page) <b>Unclassified</b>		21. No. of Pages <b>40</b>	22. Price* <b>A03</b>

\* For sale by the National Technical Information Service, Springfield, Virginia 22161

National Aeronautics and  
Space Administration

THIRD-CLASS BULK RATE

Postage and Fees Paid  
National Aeronautics and  
Space Administration  
NASA-451



Washington, D.C.  
20546

Official Business

Penalty for Private Use, \$300

2 1 1U, A, 052078 S00903DS  
DEPT OF THE AIR FORCE  
AF WEAPONS LABORATORY  
ATTN: TECHNICAL LIBRARY (SUL)  
KIRTLAND AFB NM 87117

**NASA**

POSTMASTER: If Undeliverable (Section 158  
Postal Manual) Do Not Return

---